12-14-2021

Electrochemical Beacon Method to Quantify 10 Attomolar Nucleic Acids with a Semilog Dynamic Range of 7 Orders of Magnitude

Rahul Tevatia

Alicia Chan

Lance Oltmanns

Jau Min Lim

Ander Christensen

See next page for additional authors

Authors

Rahul Tevatia, Alicia Chan, Lance Oltmanns, Jau Min Lim, Ander Christensen, Michael Stroller, and Ravi Saraf

HHS Public Access

Author manuscript

Anal Chem. Author manuscript; available in PMC 2022 August 17.

Published in final edited form as:

Anal Chem. 2021 December 14; 93(49): 16409–16416. doi:10.1021/acs.analchem.1c03020.

Electrochemical Beacon Method to Quantify 10 Attomolar Nucleic Acids with a Semilog Dynamic Range of 7 Orders of Magnitude

Rahul Tevatia,
Vajra Instruments, Lincoln, Nebraska 68512, United States

Alicia Chan,
Vajra Instruments, Lincoln, Nebraska 68512, United States

Lance Oltmanns,
Vajra Instruments, Lincoln, Nebraska 68512, United States

Jay Min Lim,
Vajra Instruments, Lincoln, Nebraska 68512, United States

Ander Christensen,
Vajra Instruments, Lincoln, Nebraska 68512, United States

Michael Stoller,
Vajra Instruments, Lincoln, Nebraska 68512, United States

Ravi F. Saraf
University of Nebraska, Lincoln, Nebraska 68588, United States; Nebraska Center for Material and Nanoscience, University of Nebraska-Lincoln, Lincoln, Nebraska 68588, United States

Abstract

Change in the dynamics of single-stranded DNA or RNA probes tethered to an Au electrode on immunospecific binding to the analyte is a versatile approach to quantify a variety of molecules, such as heavy metal ions, pesticides, proteins, and nucleic acids (NAs). A widely studied approach is the electrochemical beacon method where the redox of a dye attached to the probe decreases as its proximity to the underlying electrode changes on binding. The limit of quantification (LOQ) defined by the semilog dependence of the signal on target concentration is in the picomolar range. Here, a method was studied where, by differential reflectivity, multiple reactions were measured on a monolith electrode. An alternative contrast mechanism was discovered, which led to an approach to enhance the LOQ to 10 aM and increase the dynamic range to 7 orders of magnitude

Corresponding Authors: Rahul Tevatia – Vajra Instruments, Lincoln, Nebraska 68512, United States; rahul.tevatia@vajrainstruments.com, **Ravi F. Saraf** – University of Nebraska, Lincoln, Nebraska 68588, United States; Nebraska Center for Material and Nanoscience, University of Nebraska-Lincoln, Lincoln, Nebraska 68588, United States; rsaraf2@unl.edu.

Supporting Information

The Supporting Information is available free of charge at https://pubs.acs.org/doi/10.1021/acs.analchem.1c03020.
Details on chip spotting, probe and target sequences, SEED setup and signal, optimization of MCH backfilling (DPV and SEED) and prehybridization, effect of binding time, signals to specific binding, and sensitivity analysis of prehybridization on different GC fraction sequences (PDF)

using similar probes and binding conditions. Quantitative analysis on sequences with the *G–C* fraction ranging from 37 to 72% was performed. The approach will allow for the development of a label-free, enzyme-free microarray to detect biomolecules including NAs and proteins on a single electrode at quantification from 10 aM to 0.1 nM with high specificity.

Graphical Abstract

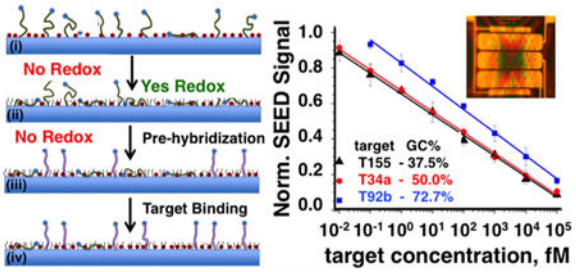

SUMMARY

In summary, we have proposed a strategy to improve the performance of the electrochemical beacon method by prehybridization to achieve a LOQ of 10 aM and a dynamic range of 7 orders of magnitude. For the study, ~25 nucleotide probes of ssDNA with MB at 3′-end were tethered on the Au electrode at the 5′ end via thio linkage followed by backfilling with MCH. The binding with similar lengths of the target was measured as a decrease in the redox peak of tethered MB. The prehybridization approach was based on two observations: first, for no backfilling, there was no MB redox even though there was complete accessibility to the underlying Au electrode. Second, the MB redox strongly depends on the probe sequence. The results suggest that the MB redox exclusively occurs when the chain is adsorbed to the surface due to strong interaction between the bases and Au. On binding, if the probe is already standing up, no change in the signal will occur. However, if the probe is adsorbed the interaction with the base is broken and the duplex stands up resulting in a decrease in the signal. Therefore, the strategy was to prime the chip by prehybridizing with a large amount of a specific target so that the probes standing up will bind first leaving only the adsorbed probes. As a result, when the targets bind to a prehybridized chip, the redox signal changes significantly with only 10 aM target concentration compared to nanomolars for a similar change in the chip that was not primed. The redox of MB was measured by a home-built differential reflectometer called SEED that allowed reading on multiple 10 μm spots on a monolith electrode. An LOQ and dynamic range of 10 aM and 7 orders of magnitudes were obtained for a *G–C* fraction of up to 50%. The LOQ reduced to 100 aM for a *G–C* fraction of 72%. Based on the combination of prehybridization with multiplexing on a monolith electrode by SEED, the findings will allow the development of label-free, enzyme-free, electrochemical DNA and RNA probe microarray chip technology to quantify a variety of molecules including NAs and proteins on a monolith electrode in the aM to picomolar range.

INTRODUCTION

Single-stranded DNA (ssDNA) tethered to an Au electrode is a broad platform to develop highly specific electrochemical biosensors for a wide range of analytes by measuring the change in the interfacial property on binding.[1,2] One pervasively studied principle is to

detect the analyte by measuring the change in the molecular dynamics of the tethered ssDNA on binding.[3–5] The concept is a highly versatile platform where the ssDNA sequence of the "DNA brush" can be engineered with complexities, such as aptamers with hairpins,[6–8] to target small analytes, such as heavy ions[9–11] and organophosphorus pesticides,[12,13] to larger biomolecules, such as the HER2 protein for breast cancer screening,[14] thrombin and cocaine,[15] interferon-gamma,[16] SARS-CoV-2 spike glycoprotein,[17] and circulating biomolecules in blood.[18,19] The change in chain dynamics can be conveniently measured as an active electrochemical signal by attaching a redox-active compound, such as methylene blue (MB)[20] or ferrocene (Fc),[21] to the free-end of the probe ssDNA. Because the electrochemical signal of binding depends on the proximity and accessibility of the redox reporter to the electrode, the platform strategy is referred to as the "electrochemical beacon".[22]

In the simplest configuration, the fully unfolded probes are 10 to 50 nucleotide (nt) long and are usually modified at the 5′ end with a thio group via a flexible spacer, for example, HS− $(CH_2)_6$− [ssDNA]-3′, that can spontaneously bind to the Au electrode via a strong Au–S bond. The alkyl chain spacer provides the flexibility to enable efficient binding to the analyte.[23,24] The typical coverage of the probes on the Au electrode is around 5×10^{12} molecules/cm^2, amounting to an interchain spacing of ~4.5 nm, which is comparable to the end-to-end distance of the probe which, for example, is ~5.5 nm for the 40 nt chain.[25] Considering the footprint to be about the size of the persistence length of ~1.5 nm,[25] the remaining well over 50% of the area is passivated with an inert compound, the most popular one being mercaptohexanol (MCH).[26] With a fluorophore attached at the free-end of the probe ssDNA, a significant change in chain flexibility occurs that was leveraged to measure probe-target binding at a sensitivity of 10 pM.[27,28] In an electrochemical analogue, a systematic decrease in the redox signal of Fc and MB tethered at the free-end is leveraged to quantify binding of target nucleic acid (NA) also as low as ~10 pM.[3,4,29]

The balance between coverage and its effect on the conformation and accessibility of probe, and ultimately the binding efficiency is delicate. Typically, coverage in the DNA brush biosensor is from 10^{11} to 10^{13} probe molecules/cm^2,[4,5] where the interchain distance is 30 to 3 nm, respectively, which at higher coverage is comparable to their size.[25,30] Several studies have shown that higher coverage, typically above 10^{13} molecules/cm^2, leads to lower binding efficiency, attributed to steric hindrance and electrostatic repulsion.[31–34] Thus, a coverage of around 5×10^{12} molecules/cm^2 seems optimal.

The primary motivation to study this highly versatile electrochemical beacon sensing method is to improve its limit of quantification (LOQ) and dynamic range. As noted above, the binding efficiency drops significantly above ~10^{13} molecules/cm^2. As a result, the LOQ for current methods is limited to the nanomolar range to at most tens of the picomolar range.[3,28,29,35] Nonlinear systematics of up to 1 fM is possible using a complex configuration with highly folded probe ssDNA.[36] The dynamic range is typically less than 3 orders of magnitude,[35] which may be increased to 5 orders of magnitude using a complex sandwich structure.[37] Considering the largely ignored aspects of the interaction between the ssDNA probe and the Au electrode and the effect of backfilling, we discovered inevitable heterogeneous conformational states of the probe where not all binding will lead to a

change (i.e., decrease) in the redox signal. By regulating the heterogeneity of the probe conformation, we demonstrate that the LOQ can be enhanced by 6 orders of magnitude to 10 aM and obtain a dynamic range of 7 orders of magnitude. Furthermore, the approach to measure the redox allows easy multiplexing by measuring multiple redox reactions on a monolith electrode with a measurement spot diameter of ~10 μm and sample volume of ~100 μL.

EXPERIMENTAL SECTION

Reagents and Buffers.

Ultrapure DNase/RNase free water (Thermo Fischer Scientific, USA) was used to prepare all buffer solutions and other solutions, subsequently referred to as DI water. Prehybridization, hybridization, and scanning electrometer for electrical double-layer (SEED) analysis were done in 1X-MPBS (1 M NaCl; 10 mM phosphate buffer, pH 7.2; 1 mM $MgCl_2$) (Sigma-Aldrich, USA). Probes with tethered MB and thiol groups (Supporting Information, Table S1) and targets (Supporting Information, Table S2) were purchased from Integrated DNA Technologies (IDT), USA. High purity 6-mercapto-1-hexanol (MCH) was purchased from Sigma-Aldrich, USA.

Chip Fabrication.

Si chips (1 cm^2) with ~1000 nm thermal oxide with three Au electrodes (thickness 300 nm; dimensions 0.1 × 0.8 mm) were patterned for 200 μm diameter microwells (n = 25) (Supporting Information, Figure S1) using a positive photoresist, KL 5315 (KemLabs, USA) lithography. Briefly, the chips were cleaned by sonication for 5 min each in acetone, water, and ethanol, followed by O_2 plasma (at 500 mTorr, 125 W) for 2 min. The chips were blow-dried by compressed air through a 0.2 μm Millipore filter. The positive photoresist was spin-cast on the chips at 5000 rpm for 60 s to obtain a ~500 nm thick film. The chips were prebaked for 5 min at 115 °C. The film was exposed to xenon (Xe) light (300 W) for 3 min through a contact mask with a chromium (Cr) metalized pattern on quartz using a mask aligner (Suss MJB3, Karl Suss, USA). The chips were developed in tetramethylammonium hydroxide developer solution by sonication for 5 min followed by a ~60 s wash in DI water. The chips were then exposed to O_2 plasma (60 W for 2 min) and hard baked at 180 °C for 1 h. The resulting pattern on each electrode was an array of 200 μm microwells exposing the underlying Au electrode.

Probe Immobilization.

Typically, unless otherwise noted, 10 μM probes (Supporting Information, Table S1) in 1 M phosphate buffer, pH 7.2 (Sigma-Aldrich, USA) immobilized the lithographed chips. In certain cases, the concentration was varied (Figure 1c) but the buffer was the same. The spotted chips with respective ~100 nL of probe solutions were allowed to incubate in a humid environment at 21 °C for about 90 min to ensure that the drop does not evaporate or grow due to condensation. After immobilization, the chip was washed in 1 mM Tris-Cl, pH 7.2.

Probe Coverage.

The method to measure probe coverage is described in detail in a previous publication.[38] Briefly, all 75 microwells were immobilized with a single concentration of P34a as described above (Probe immobilization). The probes were striped by applying −1.0 V for 10 min in phosphate buffer. The stripped probes were quantified using qPCR.

MCH Backfilling.

Typically, a solution of 0.1 mM MCH was prepared in 1 mM Tris-Cl buffer for backfilling. The immobilized chips were washed in 1 mM Tris-Cl buffer for 5 min and immersed in MCH solution for 10 min under constant stirring. The chips were then washed in 1 mM Tris-Cl buffer for 5 min. To study the effect of backfilling, MCH concentrations were changed from 0 (no backfilling) to 2.5 mM in the same buffer.

Scanning Electrometer for the Electrical Double Layer.

The primary electrochemical analysis was performed by SEED as briefly described in Supporting Information, Section S3 and Figure S2 (Vajra Instruments, USA). The CV ramp for SEED was −0.5 to +0.1 V at a scan rate of 1 V/s and step size of 24 mV with respect to a Ag/AgCl reference electrode. A periodic AC potential of frequency, ω = 500 Hz, at an amplitude of 100 mV was added to the CV ramp. The raw data were acquired by in-house software in Python scripts. The data were analyzed by MATLAB software (MathWorks, USA). The mathematical model, optical setup, and electronics instrumentation are described in a previous publication.[38]

Hybridization.

The binding to probes (Supporting Information, Table S1) with specific and nonspecific targets (Supporting Information, Table S2) was performed in 1X-MPBS at room temperature. Typically, the generic nonspecific probe for control was Pcel39a. The specific probes and targets are noted in the respective parts of the study, for example, P34a and P155 in Figure 4a and 20 nM T34a for prehybridization in Figure 6. A separate chip was used for each T34a concentration of 0.01 fM to 100 pM. For prehybridization and post-prehybridization, the binding time was 60 and 180 min, respectively. The chips were washed in fresh 1X-MPBS to remove the adsorbed/unbound target molecules.

RESULTS AND DISCUSSION

An array of 25 microwells of 200 μm diameter were patterned on each of the three Au electrodes of a 1 cm^2 chip by photolithography (see the Experimental Section). The ssDNA probes were spotted on each microwell using a home-built spotter, where the volume of the probe solution droplet of ~0.5 nL and alignment on the microwell were spontaneously controlled by surface tension (Supporting Information, Figure S1). The probes with an −SH terminal were immobilized onto the electrode via well-known Au–S bond by incubation for 90 min in a humid environment at 21 °C to ensure no evaporation of the drop during the process (see the Experimental Section). The probes had the generic formula of 3′-MB-[DNA]−$(CH_2)_6$−SH (Supporting Information, Table S1). The ssDNA sequences for the study emulates miRNA circulating in the human blood that are promising biomarkers for

early detection of cancer as referenced in Supporting Information, Table S1. For example, probe, P34a, is the DNA equivalent of complement to miR34a where uracil is replaced with thymine bases. Three specific target sequences, miR155, 34a, and 92b were selected for the study (Supporting Information, Table S2). The sequences chosen covered the typical range of the GC fraction of 35–70% typically found in human miRNA.[39] Subsequently, the chip was backfilled using MCH to passivate the exposed Au electrode. The primary study is on miR34a using a specific target, T34a.

The local redox of tethered MB on each microwell was measured by differential reflectivity of a ~10 μm diameter laser beam during cyclic voltammetry (CV). The principle and setup of the home-built reflectometer called SEED described earlier[38] is outlined in Supporting Information, Section S3 and Figure S2. Briefly, in SEED, a small AC potential of 100 mV amplitude at frequency, ω = 500 Hz, was applied as the CV potential, E is periodically ramped between −0.5 and 0.1 V relative to the Ag/AgCl reference electrode. The signal from SEED is the amplitude of reflectivity R oscillating at ω, as the E is cycled over time, t (Supporting Information, Figure S3). The response for all the roughly eight CV cycles was superimposed to obtain an average $\langle R \rangle$ as a function of E, and the error halo was due to small cycle-to-cycle variations (Figure 1a). The peaks in $\langle R \rangle$ (and R) correspond to oxidation and reduction of MB. Due to the rapid exchange of electrons with the electrode compared to the slow diffusion of ions to compensate the imbalance, the electrical double layer is unable to screen the charge leading to enhancement in ion oscillation causing the peaks.[38,40] As the higher order harmonics at 2ω was 10^3-fold lower, the system was linear. Thus, from electrostatics[38] and also confirmed experimentally, the peak $\langle R \rangle$, R_{max}, scales linearly with the peak current, I_{max}.[38,41] As MB reduces to leucomethylene blue, for this study, we chose the reduction peak for R_{max}. The spot-to-spot variation between the three electrodes on the chip was small indicating fairly uniform coverage by individual spotting (Figure 1b). As expected, the R_{max} and probe coverage increased with probe concentration (Figure 1c). For the probe coverage, the Au–S bond were electrochemically cleaved, and the absolute copy number was determined by quantitative PCR (qPCR) as described in an earlier study.[38] A probe concentration of 10 μM was used in the study that yielded fairly stable R_{max} (being in the plateau region) with a coverage of ~6×10^{12} ssDNA/cm^2.

The effect of MCH concentration on backfilling revealed unexpected and surprising results that became the genesis of this study, leading to a strategy to improve the LOQ. Three probes of different GC fractions from 37.5 to 72.7% were immobilized individually on 25 microwells of each of the three respective electrodes of the chip. The backfilling was regulated by changing the MCH concentration for a fixed exposure time of 10 min in a well-stirred solution. For robust statistics, one spot on each microwell was measured to obtain 25 readings of R_{max} for each sequence. The R_{max} as a function of MCH concentration had two salient observations (Figure 2a). First, surprisingly, on no backfilling, that is, an MCH concentration of zero, R_{max} was zero irrespective of the sequence (Figure 2a). Typical $\langle R \rangle$ for just the MB reduction for various MCH concentrations clearly shows that for no backfilling, there was no redox peak for MB (Figure 2b). Other sequences show similar behavior (Supporting Information, Figure S4). Differential pulse voltammetry (DPV) also shows no redox at no backfilling (Supporting Information, Figure S5). As per the prevailing explanation of the electrochemical beacon, if there is no backfilling, MB at the free end

should undergo redox with no hinderance.[5,35] Second, which is not an intuitive observation, there is a significant dependence on the sequence. As the GC fraction increases, the R_{max} generally increases. As all the three chains are of similar length, the chain flexibility should not change significantly due to differences in the sequences; thus, based on a prevailing mechanism, there should not be a significant difference. The GC fraction effect was further explored by including six other sequences (see Supporting Information, Table S1) to find a systematic trend (Figure 2c) for backfilling with an MCH concentration of 0.1 mM.

An optimum MCH concentration for backfilling for our fixed backfilling process time of 10 min was in the 0.01–0.5 mM range where R_{max} is reasonably constant (Figure 2a and Supporting Information, Figure S5). We fixed the MCH concentration at 0.1 mM for the study. At higher concentrations, due to higher backfilling density, overcrowding effects occur leading to a decrease in R_{max} (Figure 2a) and DPV (Supporting Information, Figure S5). We note that although conventional electrochemical characterizations, such as CV, DPV, and AC Voltammetry, are quantitatively consistent with SEED,[38,41–43] we (currently) do not understand the absence of the peak at 1 μM in DPV (Supporting Information, Figure S5) as observed in SEED (Figure 2a).

To explain the unexpected observations, we start by considering the electrochemical potential of the system as it undergoes various surface modifications. A convenient visual approach is to consider the Fermi level (FL) or the energy, U, of the negative charge (usually electron), that is, as the system charges negatively, the FL will rise (Figure 3a). The FL and electrochemical potential are equivalent.[44] For convenience, the buffer is grounded, which is typically the case in electrochemical measurements (Figure 3a): (i) before contact, the FL of Au is lower due its high work function. The difference in the FL before contact is the PZC.[43,45] (ii) As the Au electrode is immersed in the buffer solution containing ssDNA probe with MB, the FL of the electrode rises by accumulating negative charge.[45] Owing to their higher concentration and mobility, the buffer anions accumulate more to bring the FL to equilibrium. As a result, even though the negatively charged tethered ssDNA probes are in the vicinity, most of them will stand up as the FL is already in equilibrium due to the anions from the buffer. (iii) On MCH backfilling, a majority of the buffer anions are displaced due to the strong Au–S bond of MCH. As a result, the negatively charged ssDNA will commence to come down to compensate for the loss in charge to stay in equilibrium. As a result, there will be a distribution where most probes are still up while some will be down. We note here that although this distribution should come to an equilibrium, in our experience it is very slow, usually over a day; thus, the system is usually “frustrated” with a large variation (as will be described later in Figure 4b). (iv) If an external potential, E, relative to the buffer is applied, the FL of the Au electrode will shift. For $E > 0$, past the PZC (i.e., $E > \phi$), the electrode will move down shedding all the anions and consequently repelling the ssDNA probe to stand up. As a result, with the PZC for the Au electrode at ~+0.3 V relative to Ag/AgCl,[43,45] the probes will stand up.

To explain the unexpected observations in Figure 2 in terms of electrostatics (Figure 3a), we propose that MB at the free end undergoes redox only when the ssDNA probe is adsorbed on the Au electrode [schematically indicated in Figure 3a(iii)]. The conjecture that redox of MB only occurs when the chains are down is supported by two observations: first, it is consistent

with no signal for no back filling (Figure 2a,b and Supporting Information, Figure S5) when most of the chains are up [Figure 3a(ii)]. Second, on application of +0.5 V, that is, $E > 0$, the chains will stand up [Figure 3a(iv)], causing a decrease in the redox signal of MB (Figure 3b). Furthermore, as −0.5 V was applied, that is, $E < 0$, the chains will come down again [Figure 3a(iv)], explaining the reversion to the original value. Next, building on the proposed mechanism for MB redox, we developed the electrochemical beacon method for the simplest configuration where the target is nominally the same size as the probe.

We tested for specificity, as it is the minimum requirement to measure biospecimens. For a chip with P34a and P155 probes on the same electrode, we tested the binding to a 100 nM T34a target. The redox of MB for specific binding vanished, while for the nonspecific probe the signal was unchanged indicating no binding (Figure 4a). Thus, the specificity is high. The decrease in R_{max} on binding is explained as follows: before binding, the signal is from the probes that are down. These probes are adsorbed on the electrode due to the well-documented strong interaction between Au and the bases.[46,47] On probe-target binding, the bases will unbind from Au as they are folded inside the double helix. Due to the thermal motion of the rigid dsDNA, the anions from the solution will replace the charge on the electrode to compensate for the (lost) negative charge from the probe ssDNA. As a result, the chain will stand up on binding. Thus, on binding, the redox signal will vanish causing the overall signal to drop. As the interaction of bases with Au depends on the sequence,[46,47] this mechanism also qualitatively explains the GC dependence on the R_{max} shown in Figure 2c.

The relative decrease in R_{max} before (R_O) and after binding (R_B) was studied as a function of the target concentration, T34a (Figure 4b). The length of T34a is similar to that of P34a (Supporting Information, Table S1). For a binding time of 60 min, an insignificant change in the redox signal was observed at target concentrations below 10 nM. Thereafter, the signal decreases rapidly. Importantly, the decreases in the R_B/R_O exhibited a significant scatter with no particular systematics with respect to the GC fraction as was the case before binding (in Figure 2). Each data point for a 60 min binding time was averaged over three readings on different microwells with R_B and R_O measured on the same respective microwell. Furthermore, the characteristics for a binding time of 120 min was similar, including the large scatter (data points shown in Supporting Information, Figure S6). The proposed mechanism points to an intrinsic challenge: As the probes that are up would be more prone to binding but will lead to no change in the redox signal. A change (i.e., decrease) in R_{max} will occur only when the binding is with chains that are down. As the majority of probes are up [Figure 3a(iii)], the threshold to affect change in the signal required a large concentration of the target (Figure 4b). As the distribution of up versus down probe chains was difficult to control, as noted above as “frustrated distribution” in Figure 3a(iii), due to slow kinetics, the change in the signal was noisy (Figure 4b and Supporting Information, Figure S6).

We propose a simple, novel strategy of a “prehybridization” step to leave only adsorbed probes bound to the target; as a result, both the sensitivity will be improved and the scatter will be reduced. The process is as follows (Figure 5): based on the proposed mechanism [Figure 3a(ii)], after immobilization very few probes are down [i.e., schematically, only P7 in Figure 5(i)] leading to $R_{max} = 0$ (Figure 2a). On MCH backfilling, the anions of the

solution are displaced by MCH, causing some chains to come down [Figure 3a(iii)], which are schematically represented as P4, P6, P7, and P9 [Figure 5(ii)]. On prehybridization with a large enough number of specific targets, all the probes standing up, that is, P2, P3, P5, and P8, will bind [Figure 5(ii)]. Owing to the large scatter of up/down distribution, the concentration of the target for prehybridization will be beyond the threshold, for example, 20 nM (Figure 4b). Few adsorbed targets, such as P9, will also bind and stand up during prehybridization [Figure 5(iii)]. The optimization of prehybridization step (Supporting Information, Figure S7) indicates that 20 nM specific target for 1 h is sufficient to hybridize all up probe chains [Figure 5(iii)]. Now the chip is primed to bind to the target where the only probes available for binding are all down. As a result, the targets will exclusively bind to probes that are down (such as P6 and P7), resulting in a decrease in the redox signal as the duplex stands up [Figure 5(iv)].

The concept is illustrated for binding with a 0.1 fM T34a target to the immobilized probe P34a. Two conditions are compared, where the probes on one electrode are directly exposed to the target versus the probes on the other electrode (on the same chip) are primed by prehybridization before target binding (Figure 6a). For the probes not subject to prehybridization, consistent with previously reported methods,[3,28,29,35] no change in R_{max} occurred. However, when the probe was prehybridized with 20 nM target there was a remarkable change in the signal by ~30% due to binding with the 0.1 fM target. The prehybridization concentration being above the threshold (Figure 4b) leaves probes that adsorbed [as in Figure 5(iii)], which leads to change in the signal even with the 0.1 fM target. As a comparison, the ~30% drop in the prehybridized chip by the 0.1 fM target (Figure 6a) is equivalent to a 20 nM target required for the same drop without prehybridization (Figure 4b). Thus, prehybridization improves the sensitivity by 8 orders of magnitude.

Next, we consider quantification. The large variation in R_{max} after prehybridization, that is, R_B, is inevitable (i.e., Figure 4b). The large scatter in R_B occurs in spite of the initial fairly uniform distribution of up versus down probes before binding (i.e., Figure 1b). However, if the number of probes that are adsorbed are sufficient after prehybridization, that is, $R_B \sim 1 \times 10^{-4}$ (as in Figure 6a), we have adequate range to engineer a viable quantitative method. To compensate for the large scatter in R_{max} after prehybridization (i.e., R_B), the R_{max} on subsequent binding to the target (post-prehybridization), R_f, was normalized as R_f/R_B. To study the effect of the sequence, three sequences covering *G*–*C* fractions from 37.5 to 72.7% were studied (Figure 6b). The $\langle R \rangle$ normalized by R_B was well above the noise level for a broad target concentration. Typical normalized $\langle R \rangle$ showing a systematic change on binding for all the three sequences is shown in the Supporting Information for each of the target concentrations (Supporting Information, Figure S8). R_f/R_B was quantitative, exhibiting a highly linear signal on a semilog plot over the entire range (Figure 6b). The resulting LOQ was 10 aM and the dynamic range was 7 orders of magnitude. Each data point was averaged over six microwells on the same chip. The error bars were very small. The chip also had control on each of the electrodes with probes that were nonspecific to the target to ensure specificity. The nonspecific probes for T34a were P155, P92b, and Pcel39a, while for the other two targets the controls were the (other) two noncomplementary probes and Pcel39a. We note that at a high *G*–*C*% of 72%, that is, P92b, the LOQ was 100 aM. We conjecture

that the lower LOQ was due to poor binding efficiency owing to the strong adsorption of the probe to the Au electrode due to the high *G–C* fraction (Figure 2c). To quantify the change in binding efficiency on the *G–C* fraction, unfortunately, the binding constant, unlike for fluorescence-based systems,[48] is difficult primarily because binding to probes that are up will lead to no change in the signal, while the ones down will lead to a change in the signal [as shown in Figure 5(iii) and experimentally shown in Figure 6a]. To independently measure the binding constant for up versus down probes that will be different requires concomitant measurement of the structure in real-time to follow the kinetics. Although, the structural heterogenous complexity of the immobilized film (i.e., Figure 5) makes binding constant measurement difficult, the systematics is robust as evident from the tight error bar (Figure 6b). The calibration curve for T155 and T34a being nominally coincident suggests that below 50% *G–C* fraction, the desorption of the probe to bind is the ratedetermining step rather than the hybridization kinetics.

Supplementary Material

Refer to Web version on PubMed Central for supplementary material.

ACKNOWLEDGMENTS

R.F.S. thanks the National Cancer Institute of the National Institutes of Health, USA for financial support (2R44CA199058).

The authors declare the following competing financial interest(s): R.F.S. discloses financial interest in Vajra Instruments as its founder and officer.

REFERENCES

(1). Campuzano S; Yáñez-Sedeño P; Pingarrón JM ChemElectroChem 2019, 6, 60–72.

(2). Pellitero MA; Shaver A; Arroyo-Currás N J. Electrochem. Soc 2020, 167, 037529.

(3). Fan C; Plaxco KW; Heeger AJ Proc. Natl. Acad. Sci. U.S.A 2003, 100, 9134–9137. [PubMed: 12867594]

(4). Idili A; Amodio A; Vidonis M; Feinberg-Somerson J; Castronovo M; Ricci F Anal. Chem 2014, 86, 9013–9019. [PubMed: 24947124]

(5). Dauphin-Ducharme P; Arroyo-Currás N; Plaxco KW J. Am. Chem. Soc 2019, 141, 1304–1311. [PubMed: 30605323]

(6). Han K; Liang Z; Zhou N Sensors) 2010, 10, 4541–4557. [PubMed: 22399891]

(7). Hai X; Li Y; Zhu C; Song W; Cao J; Bi S Trends Anal. Chem 2020, 133, 116098.

(8). Yoo H; Jo H; Oh SS Mater. Adv 2020, 1, 2663–2687.

(9). Wang L; Peng X; Fu H; Huang C; Li Y; Liu Z Biosens. Bioelectron 2020, 147, 111777. [PubMed: 31634804]

(10). Yang Y; Li W; Liu J Anal. Chim. Acta 2021, 1147, 124–143. [PubMed: 33485571]

(11). Abu-Ali H; Nabok A; Smith T Chemosensors 2019, 7, 27.

(12). Selvolini G; Băjan I; Hosu O; Cristea C; Săndulescu R; Marrazza G Sensors 2018, 18, 2035.

(13). Phopin K; Tantimongcolwat T Sensors 2020, 20, 6809.

(14). Ferreira DC; Batistuti MR; Bachour B; Mulato M Bioelectrochemistry 2021, 137, 107586. [PubMed: 32966935]

(15). White RJ; Phares N; Lubin AA; Xiao Y; Plaxco KW Langmuir 2008, 24, 10513–10518. [PubMed: 18690727]

(16). Liu Y; Tuleouva N; Ramanculov E; Revzin A Anal. Chem 2010, 82, 8131–8136. [PubMed: 20815336]

(17). Song Y; Song J; Wei X; Huang M; Sun M; Zhu L; Lin B; Shen H; Zhu Z; Yang C Anal. Chem 2020, 92, 9895–9900. [PubMed: 32551560]

(18). Li H; Dauphin-Ducharme P; Ortega G; Plaxco KW J. Am. Chem. Soc 2017, 139, 11207–11213. [PubMed: 28712286]

(19). Li H; Arroyo-Currás N; Kang D; Ricci F; Plaxco KW J. Am. Chem. Soc 2016, 138, 15809–15812. [PubMed: 27960346]

(20). Ricci F; Lai RY; Heeger AJ; Plaxco KW; Sumner JJ Langmuir 2007, 23, 6827–6834. [PubMed: 17488132]

(21). Husken N; Gebala M; Schuhmann W; Metzler-Nolte N Chembiochem 2010, 11, 1754–1761. [PubMed: 20602405]

(22). Radi A-E; Acero Sánchez JL; Baldrich E; O'Sullivan CK J. Am. Chem. Soc 2006, 128, 117–124. [PubMed: 16390138]

(23). Southern E; Mir K; Shchepinov M Nat. Genet 1999, 21, 5–9. [PubMed: 9915493]

(24). Peeters S; Stakenborg T; Reekmans G; Laureyn W; Lagae L; Van Aerschot A; Van Ranst M Biosens. Bioelectron 2008, 24, 72–77. [PubMed: 18440798]

(25). Chen H; Meisburger SP; Pabit SA; Sutton JL; Webb WW; Pollack L Proc. Natl. Acad. Sci. U.S.A 2012, 109, 799–804. [PubMed: 22203973]

(26). Herne TM; Tarlov MJ J. Am. Chem. Soc 1997, 119, 8916–8920.

(27). Rant U; Arinaga K; Fujita S; Yokoyama N; Abstreiter G; Tornow M Nano Lett. 2004, 4, 2441–2445.

(28). Rant U; Arinaga K; Scherer S; Pringsheim E; Fujita S; Yokoyama N; Tornow M; Abstreiter G Proc. Natl. Acad. Sci. U.S.A 2007, 104, 17364–17369. [PubMed: 17951434]

(29). Cai Z; Song Y; Wu Y; Zhu Z; James Yang C; Chen X Biosens. Bioelectron 2013, 41, 783–788. [PubMed: 23102830]

(30). Rao AN; Grainger DW Biomater. Sci 2014, 2, 436–471. [PubMed: 24765522]

(31). Peterson AW; Heaton RJ; Georgiadis RM Nucleic Acids Res 2001, 29, 5163–5168. [PubMed: 11812850]

(32). Steel AB; Herne TM; Tarlov MJ Anal. Chem 1998, 70, 4670–4677. [PubMed: 9844566]

(33). Gong P; Levicky R Proc. Natl. Acad. Sci. U.S.A 2008, 105, 5301–5306. [PubMed: 18381819]

(34). Irving D; Gong P; Levicky RJ Phys. Chem. B 2010, 114, 7631–7640.

(35). Xiao Y; Lubin AA; Baker BR; Plaxco KW; Heeger AJ Proc. Natl. Acad. Sci. U.S.A 2006, 103, 16677–16680. [PubMed: 17065320]

(36). Wang T; Viennois E; Merlin D; Wang G Anal. Chem 2015, 87, 8173–8180. [PubMed: 26241158]

(37). Xia F; White RJ; Zuo X; Patterson A; Xiao Y; Kang D; Gong X; Plaxco KW; Heeger AJ J. Am. Chem. Soc 2010, 132, 14346–14348. [PubMed: 20873767]

(38). Tevatia R; Prasad A; Saraf RF Anal. Chem 2019, 91, 10501–10508. [PubMed: 31313582]

(39). Davis N; Biddlecom N; Hecht D; Fogel GB Comput. Biol. Chem 2008, 32, 222–226. [PubMed: 18407791]

(40). Raghunath S; Prasad A; Tevatia R; Gunther JR; Roy S; Krishnan S; Saraf RF Chemelectrochem 2018, 5, 429–433. [PubMed: 31157159]

(41). Lee S-W; Lopez J; Saraf RF Biosens. Bioelectron 2013, 47, 408–414. [PubMed: 23612062]

(42). Singh G; Moore D; Saraf RF Anal. Chem 2009, 81, 6055–6060. [PubMed: 19555111]

(43). Saraf AR; Keramatnejad K; Arcila JA; Saraf RF Adv. Mater. Interfaces 2021, 8, 2100370.

(44). Reiss HJ Phys. Chem 1985, 89, 3783–3791.

(45). Moore D; Arcila JA; Saraf RF Langmuir 2020, 36, 1864–1870. [PubMed: 32073857]

(46). Brown KA; Park S; Hamad-Schifferli KJ Phys. Chem. C 2008, 112, 7517–7521.

(47). Koo KM; Sina AAI; Carrascosa LG; Shiddiky MJA; Trau M Anal. Methods 2015, 7, 7042–7054.

(48). Zhou M; Chen X; Yang H; Fang X; Gu H; Xu H ACS Omega 2019, 4, 6931–6938.

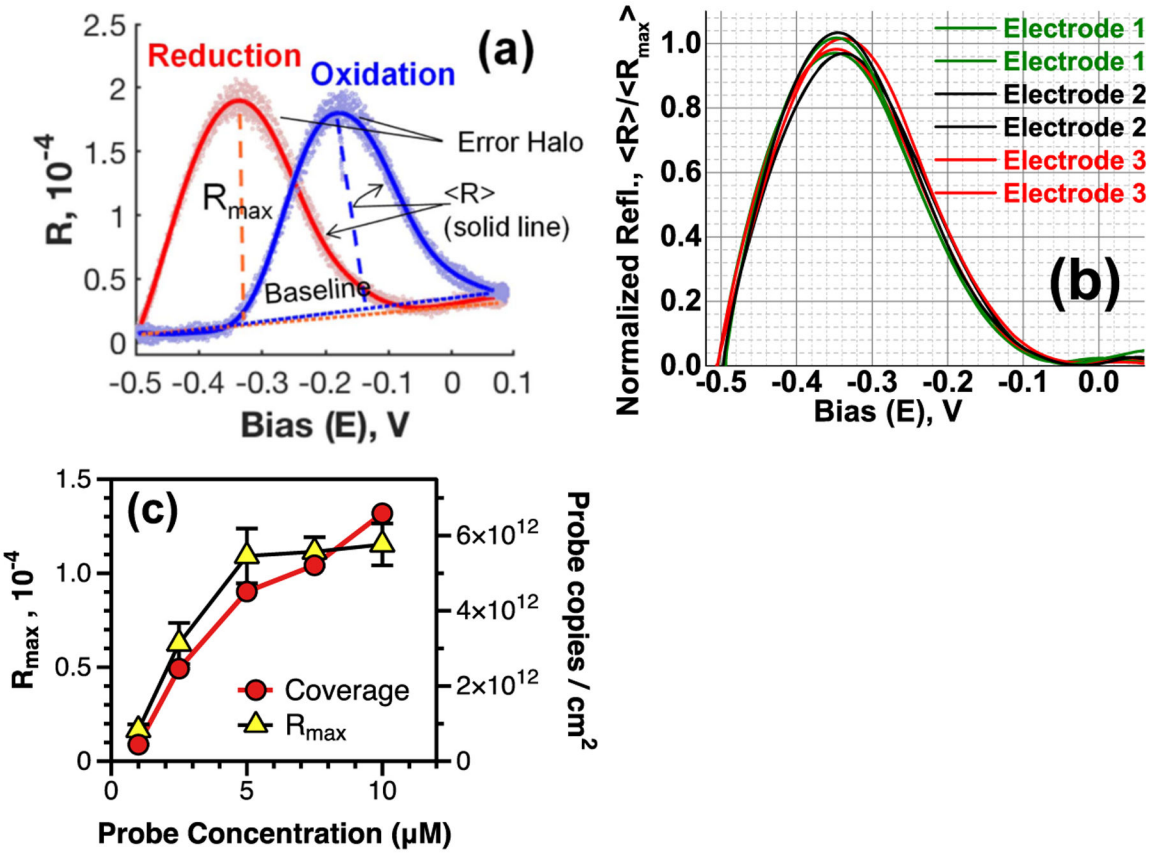

Figure 1.

SEED signal from an immobilized probe backfilled with MCH. (a) $R(E)$ for P34a immobilized at 10 μM with MCH backfilling at 1 mM. (b) Normalized $\langle R \rangle$ showing only the reduction signal at same conditions as (a) on multiple spots on a chip. (c) Effect of probe concentration on R_{max} and coverage.

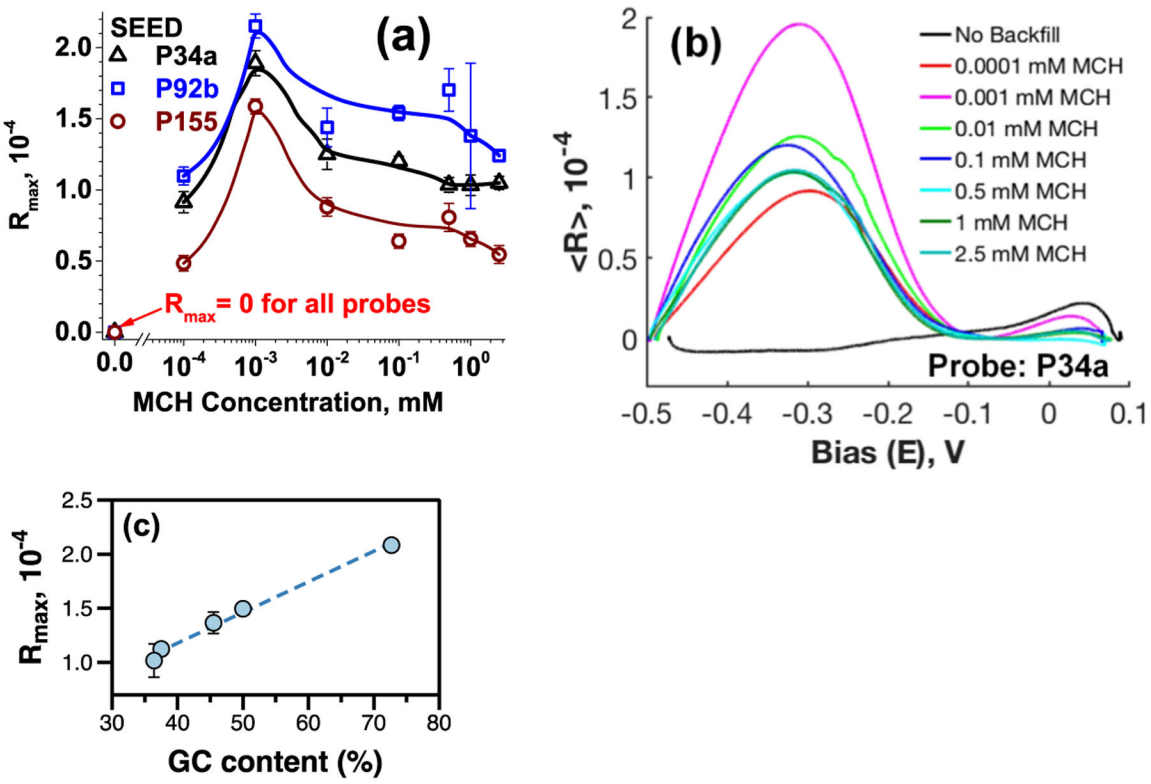

Figure 2.

Effect of MCH backfilling and the probe on R_{max}. (a) Change in R_{max} as a function of the level of backfilling regulated by MCH concentration. Note that no redox peak is observed for no backfilling. (b) Typical E versus $\langle R \rangle$ for various levels of backfilling. The data are from different chips. The $\langle R \rangle$ is corrected for baseline. (c) Effect of the sequence on the R_{max} signal at probe immobilization and backfilling conditions as Figure 1a.

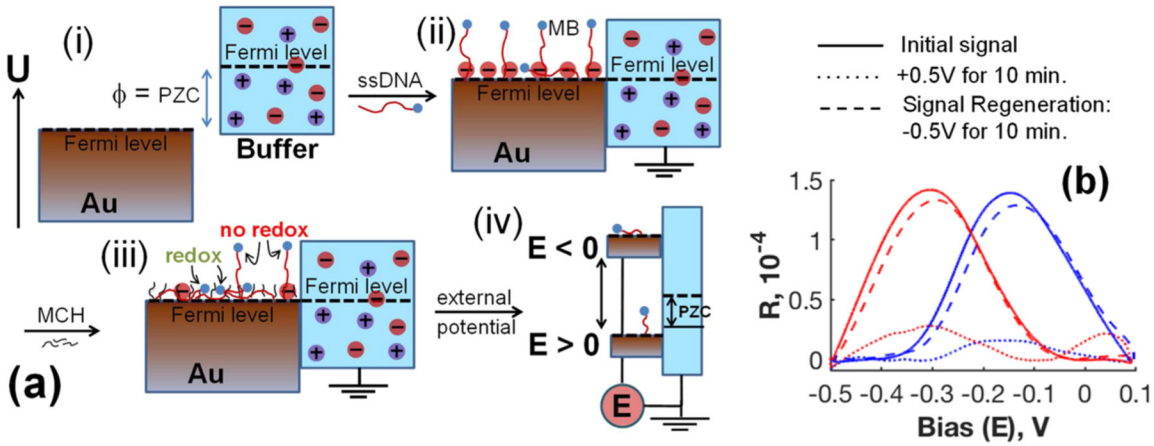

Figure 3.

State of immobilized probe due to backfilling and potential. (a) Relative FL of the electrode with respect to the electrode and change in probe conformation, (i) before electrode contacts the solution, (ii) after ssDNA probe immobilization, (iii) after backfilling, and (iv) due to external potential, *E*. The steps (ii) to (iv) are with electrode in the solution. (b) Effect of external potential on the redox signal for P34a immobilized and backfilled at conditions similar to Figure 1a. The *R* is corrected for baseline.

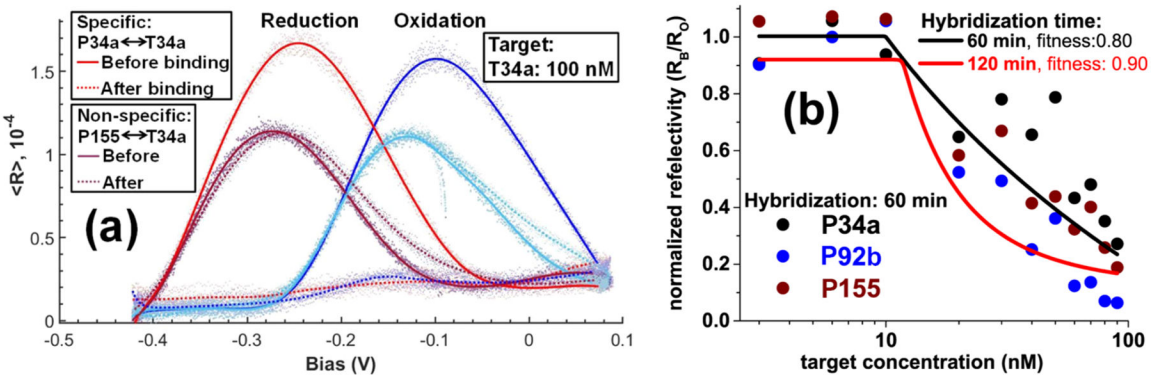

Figure 4.

Effect of high target concentration binding. (a) Change in $\langle R \rangle$ (with error halo) for P34a and P155 probes on binding to 100 nM target T34a. Both the probes are immobilized on the same electrode. The legend is for reduction peaks only. (b) Change in the reduction peak on binding to a specific target, T34a at concentration 3–100 nM. The probe immobilization and backfilling conditions are the same as Figure 1a.

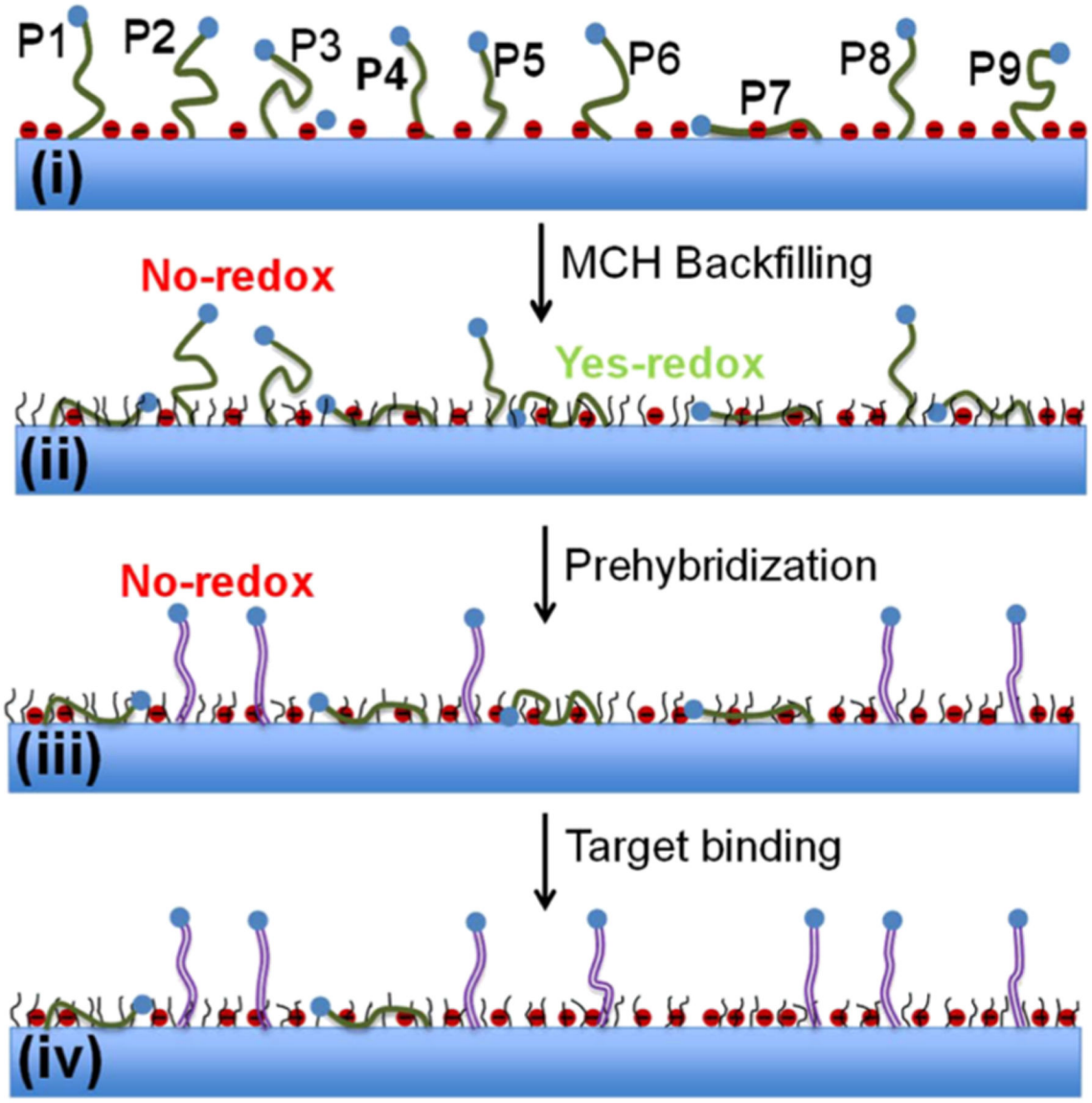

Figure 5.

Prehybridization method. Schematic representation of probe conformation from immobilization to binding. Nine probes, P1 to P9, are shown to qualitatively represent the relative fraction of conformational change. (i) Before backfilling, anions (red dots) adsorb on Au causing most probes to stand up (only P7 is down). (ii) MCH backfilling displaces the anions, bringing some of the probes down (P1, P4, P6, P7, and P9). (iii) On prehybridization all the probes up and fraction of the probes down form a duplex (P2, P3, P5, P8, and P9). (iv) Only available probes for targets to bind are down causing them to stand up (P6, P7). The probes standing up and duplex (that will all stand up) will not show MB redox according to the model.

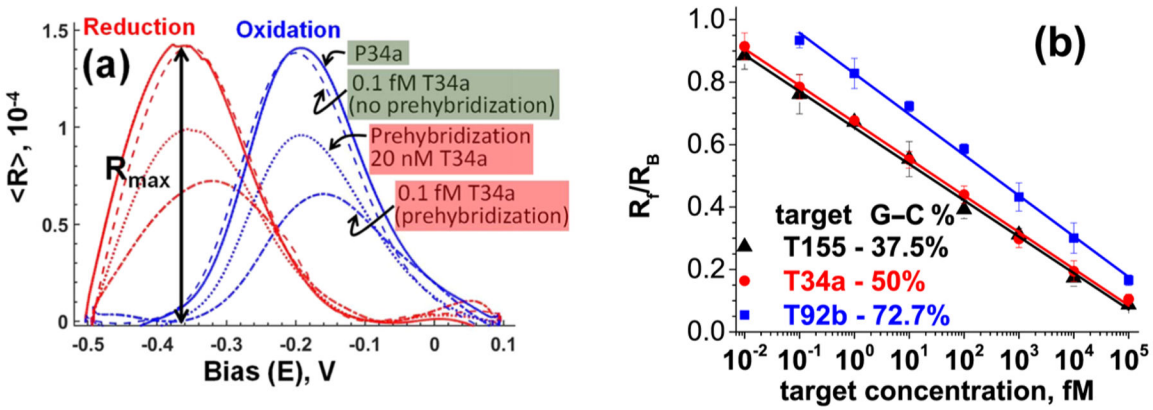

Figure 6.

Quantification of the target. (a) Effect of prehybridization showing the enhancement in sensitivity. (b) Systematic decrease in signal due to binding with the target after prehybridization. The fit for all the curves is in the 0.984–0.985 range. The error bar was based on six independent spots.